Nuclear Instruments and Methods in Physics Research B 336 (2014) 143–148

Contents lists available at ScienceDirect

Nuclear Instruments and Methods in Physics Research B

journal homepage: www.elsevier.com/locate/nimb

Experimental tests of an advanced proton-to-neutron converter at ISOLDE-CERN

A. Gottberg [a,b], T.M. Mendonca [a,c], R. Luis [d], J.P. Ramos [a,e], C. Seiffert [a,f], S. Cimmino [a], S. Marzari [a], B. Crepieux [a], V. Manea [g], R.N. Wolf [h], F. Wienholtz [h], S. Kreim [a,i], V.N. Fedosseev [a], B.A. Marsh [a], S. Rothe [a], P. Vaz [d], J.G. Marques [d], T. Stora [a,*]

[a] European Organization for Nuclear Research – CERN 1211, Geneva 23, Switzerland
[b] Consejo Nacional de Pesquisas Cientificas CSIC, Instituto de Estructura de la Materia, 28006 Madrid, Spain
[c] IFIMUP and IN – Institut of Nanosciences and Nanotechnologies, Rua do Campo Alegre 687, 4169-007 Porto, Portugal
[d] Instituto Superior Técnico, Campus Tecnológico e Nuclear – IST-CTN, Estrada Nacional 10 (km 139, 7), 2695-066 Bobadela LRS, Portugal
[e] École Polytechnique Fédérale de Lausanne – EPFL, 1015 Lausanne, Switzerland
[f] Technische Universität Darmstadt, 64289 Darmstadt, Germany
[g] CSNSM-IN2P3-CNRS, Université Paris-Sud, 91405 Orsay, France
[h] Institut für Physik, Ernst-Moritz-Arndt Universität Greifswald, 17487 Greifswald, Germany
[i] Max-Planck-Institut für Kernphysik, Saupfercheckweg 1, 69117 Heidelberg, Germany

ARTICLE INFO

Article history:
Received 21 January 2014
Received in revised form 17 April 2014
Accepted 29 April 2014
Available online 30 July 2014

Keywords:
Proton-to-neutron converter
Spallation neutron source
Isotope separation on-line (ISOL)
ISOLDE
Radioactive ion beams (RIB)

ABSTRACT

The suppression of isobaric contaminations is of growing importance for many scientific programs using radioactive isotopes produced at isotope separation on-line (ISOL) facilities, such as ISOLDE-CERN. A solid tungsten proton-to-neutron converter has been used for ten years to produce neutron-rich fission fragments from an UC_x target while suppressing the production of neutron-deficient isobaric contaminants. The remaining contamination is mainly produced by primary protons that are scattered by the heavy neutron converter and finally impinge on the UC_x target itself. Therefore, the knowledge of the energy-dependant cross-sections of proton and neutron induced fission events is crucial in order to evaluate future converter concepts.

In this paper, an improved neutron converter prototype design is presented together with the experimentally assessed radioisotope production of Rb, Zn, Cu, Ga and In that validate the converter concept aiming at beams of higher purity neutron-rich isotopes. The experimentally derived release efficiencies for isotopes produced by the 1.4 GeV protons available at ISOLDE are used to evaluate the Monte Carlo code FLUKA and the cross-section codes TALYS and ABRABLA, respectively.

1. Introduction

The next generation radioactive ion beam (RIB) facilities aim at expanding the present nuclear physics program by increasing the beam energies and intensities, enabling the study of nuclei far from stability that are otherwise difficult to produce. One of the main techniques for the production of pure and intense RIBs is the isotope separation on-line (ISOL) method. Here, a beam from a primary accelerator is used to bombard a thick target and radionuclei are produced through different reactions, such as fission, spallation and fragmentation. These isotopes are extracted from the target, ionized, electromagnetically mass-separated and distributed to the experimental apparatuses.

For an ISOL-type facility, higher beam intensities may be achieved by increasing the current of the primary beam. However, this increase has the disadvantage of augmenting the heat deposited in the target unit as well as the background of isobaric contamination of the same mass-over-charge ratio. An efficient method to cope with these limitations for neutron-rich isotopes is to induce fission by spallation neutrons. The primary proton beam is then directed to a proton-to-neutron converter, instead of the target, producing spallation neutrons that subsequently induce fission in the target material. This production method has been introduced in [1] to remove the beam power deposited in the fission target by the primary beam and to decrease the target aging. Ever since, this conversion approach has been applied at

* Corresponding author. Tel.: +41 764870808.
E-mail address: thierry.stora@cern.ch (T. Stora).

http://dx.doi.org/10.1016/j.nimb.2014.04.026
0168-583X/

the IRIS facility at PNPI [2] and ISOLDE at CERN [3], and it is also proposed for the intermediate and next-generation facilities such as SPIRAL2 at GANIL, ISAC-II at TRIUMF or EURISOL.

At the ISOLDE facility at CERN [4], more than 1000 radioactive species of more than 70 elements are produced using the ISOL method, offering unique opportunities for experiments in fundamental nuclear physics, astrophysics, solid state physics and life science.

The conventional ISOLDE neutron converter assembly, as used for the past 10 years, is based on a solid tungsten rod, as shown schematically in Fig. 1. When the beam is directed to the target (direct beam configuration) fission is induced mainly by GeV protons. When the beam is directed to the converter (converter configuration) fission, induced by the MeV energy spallation neutrons, becomes the predominant production channel, thereby decreasing the production of contaminants [3,5]. However, the present ISOLDE converter configuration results in a reduced beam intensity for the fission products compared to what is achieved for the direct beam configuration [3], which is to the largest extent a result of the poor solid angle coverage by the target of the neutrons emitted from the converter.

The standard ISOLDE target and converter configuration has been studied in detail using the Monte Carlo code FLUKA [6,7] and the cross-section codes TALYS [8] and ABRABLA [9,10]. Due to the fact that the present converter layout results in reduced ion beam intensities when compared to the direct beam configuration, alternative designs for the target system have been proposed [11]. At the same time this optimization aimed at decreasing the production of neutron-deficient species in order to improve the purity of neutron-rich-nuclear beams. To test the performance of such systems and the accuracy of theoretical modeling, a prototype target and converter system, inspired by one of the proposed configurations in [11], has been built and characterized at ISOLDE with a 1.4 GeV proton beam.

This paper reports on the development of this prototype and the results obtained during the experiment. The experimental data are compared with the simulation results obtained using FLUKA and a combination of ABRABLA and TALYS. Special attention is given to the region around the double shell closures of ^{78}Ni and ^{132}Sn. In these regions, Zn, Rb and Cs isotopes are particularly suitable for this study since they have the most appropriate release properties for the target materials presently used at ISOLDE. The data reported here validate the optimized geometry of the fission target and neutron converter for the production of purer beams of neutron-rich isotopes.

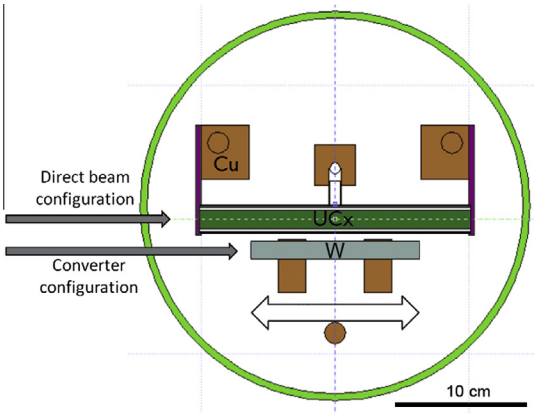

Fig. 1. Standard converter configuration of the ISOLDE target system as implemented in FLUKA.

2. Target and converter prototype design and commissioning

2.1. Numerical simulations

The two configurations shown in Fig. 2 have been proposed to improve the purity of neutron-rich isotopes beams, e.g. ^{80}Zn and ^{130}Cd, by reducing the production of neutron-deficient isobars ^{80}Rb and ^{130}Cs [11]. For both approaches an increase by more than one order of magnitude in the ratios ^{80}Zn/^{80}Rb and ^{130}Cd/^{130}Cs has been predicted. The Monte Carlo code FLUKA is used to run the simulations, with two different sets of cross-sections: FLUKA's own cross-sections and a combination of cross-sections calculated with TALYS and ABRABLA. In the later case, the average fluences (proton and neutron track-length fluence spectra) over the UC_x target volume is calculated with FLUKA; TALYS is used to compute cross-sections for energies up to 200 MeV and ABRABLA to calculate the cross-section from 200 MeV to 2 GeV, an energy range for a possible future energy upgrade connected to the HIE-ISOLDE project. More details about these numerical simulations can be found in [11].

The driving concept of the proposed change of geometry is to reduce the flux of scattered protons inside the target material container while keeping a similar compact target volume and preserving, or even increasing the flux of spallation neutrons. Common to both designs in Fig. 2 is the upstream shift (relative to the proton motion) of the uranium based target material with respect to the position of the proton-to-neutron converter.

The design finally tested at ISOLDE combines the realization of major aspects of the layout presented in the left panel of Fig. 2 with a feasible implementation into the ISOLDE target and ion source assembly. This new geometry, presented in Fig. 3, takes into account the need of a shorter UC_x container and an increased diameter of both, the container and the converter for an improvement of the production of neutron-rich species.

Thermo-electrical simulations using the ANSYS code [12] have been carried out in order to investigate the thermal behavior of the final target prototype (Fig. 3) unit under both normal operation conditions and in case of defective electrical contacts, which is a possible incident scenario. In the standard ISOLDE target units, the heating of the target container is arranged by a DC current coupled from copper connection blocks to the tantalum container via tantalum sheets, connected with stainless steel M5 screws. Fig. 4 shows the temperature distribution in the target container for an applied current of 950 A. The first simulation, shown in the upper panel of Fig. 4, is related to the normal operation conditions where no faulty contacts are found and both thermal and electrical resistance are low. The temperatures vary along the container axis since the terminals act as cold sinks, with the maximum temperature observed at the center of the container. In the lower panel of Fig. 4, the situation where the thermo-electric contacts are compromised, when they present both a limited thermal transfer coefficient of 5.0 kW m^{-2} K^{-1} and an electric conductivity of 2.7 MS m^{-2} is shown. In this case, one can observe a significant increase of the temperature in both copper blocks and tantalum sheets that can promote the formation of an intermetallic compound of stainless steel with copper with a low melting point, causing a failure of the target system.

2.2. Prototype assembly

Several design variations have been simulated before a final set of target configurations was reached (Fig. 2), constantly aiming at an optimized ratio of desired MeV spallation neutrons to unwanted scattered high-energy protons inside the target material. As modifications to these configurations several compromises had to be

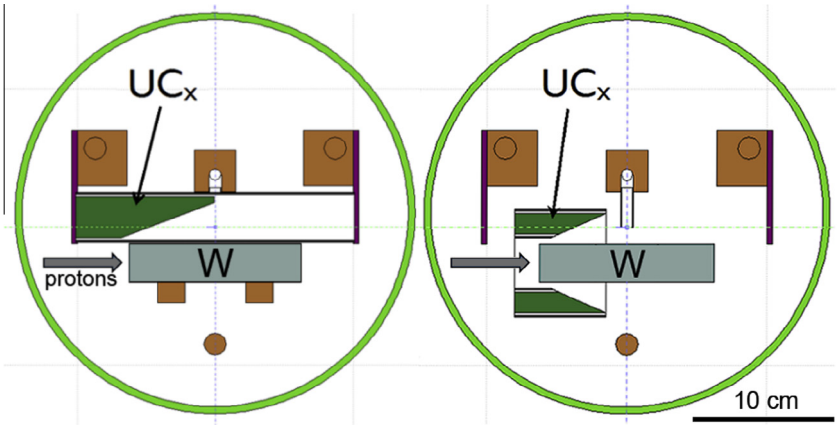

Fig. 2. Alternative configurations for the ISOLDE neutron converter and fission target system as used for simulating the production of radioisotopes [11].

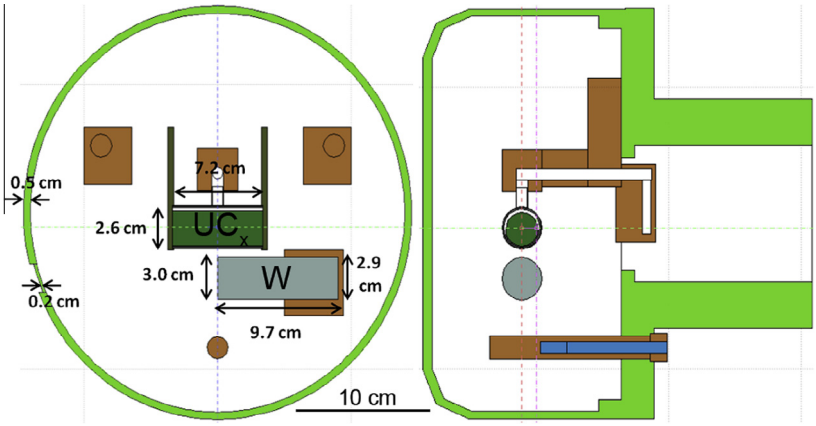

Fig. 3. Prototype converter configuration as implemented into FLUKA.

considered in order to simplify the construction of the prototype, the most important being the removal of the wedge-like cut in the UC_x target. Alike the standard units at ISOLDE, the target oven is made of tantalum and the converter of tungsten. Following the optimized geometries, the dimensions of both target and converter have been changed. The diameter of the UC_x target pellets has been increased from 1.4 to 2.6 cm and the target length set to 7.2 cm. The converter diameter has been increased from 1.2 to 3.0 cm and its length reduced from 12.5 to 9.7 cm. In addition to the changes in the dimensions, the UC_x target material and the tantalum container are centered in the unit, while the converter has been shifted in downstream direction. Furthermore, a reduction in the wall thickness of the aluminum vessel from 5 to 2 mm has been introduced at the entrance point of the proton beam. This modification has been made to further decrease the scattering of the proton beam in the aluminum vessel that would lead to an undesired increase of the proton fluence in the target material.

As described previously, in the standard units stainless steel M5 screws are used to connect the tantalum sheets to the copper blocks, used for ohmic heating of the target container. In the prototyped unit, these screws have been substituted by tantalum, since the formation of an eutectic between stainless steel and copper is otherwise likely to happen according to the simulations and observed in an early version of the prototype. Due to a different heat profile compared to conventional units and as it is observed in the thermo-electrical simulations shown in Fig. 4 the temperature at the position of these screws does not allow the use of steel.

2.3. Synthesis of uranium carbide UC_x target material

The uranium carbide target material production process has been adjusted from the standard ISOLDE procedure in order to obtain material pellets according to the non-standard geometry. As in the standard process, depleted uranium dioxide powder (0.31 at.% ^{235}U in the uranium content) is mixed with high purity synthetic graphite powder in the molar ratio of 1:6. The mixture is blended in a vibratory grinder for 20 min and pressed into pellets by employing a force of 26 tons in a stainless steel die. Forty-one of the resulting pellets with 25 mm diameter, 1.7 mm thickness and 3.0 g weight each, are piled up and inserted into a cylindrical graphite container. Carbo-thermal reduction of UO_2 is performed in vacuum of base pressure 10^{-6} mbar at temperatures up to 1820 °C where no more degassing was observed indicating no more production of CO and therefore a completion of the calcination process. The mass of the final load of 102.4 g indicates a completed reduction of UO_2 within an accuracy of 1%. Finally the material is transferred from the vacuum oven to the target unit #493, where it is inserted and sealed inside the tantalum container of the final unit as shown in Fig. 5.

3. Results and discussion

The isotope yields of copper (A = 71, 74, 75, 77), zinc (A = 74–76, 78, 80, 81), gallium (A = 80–82), rubidium (A = 80, 82, 84, 86, 88,

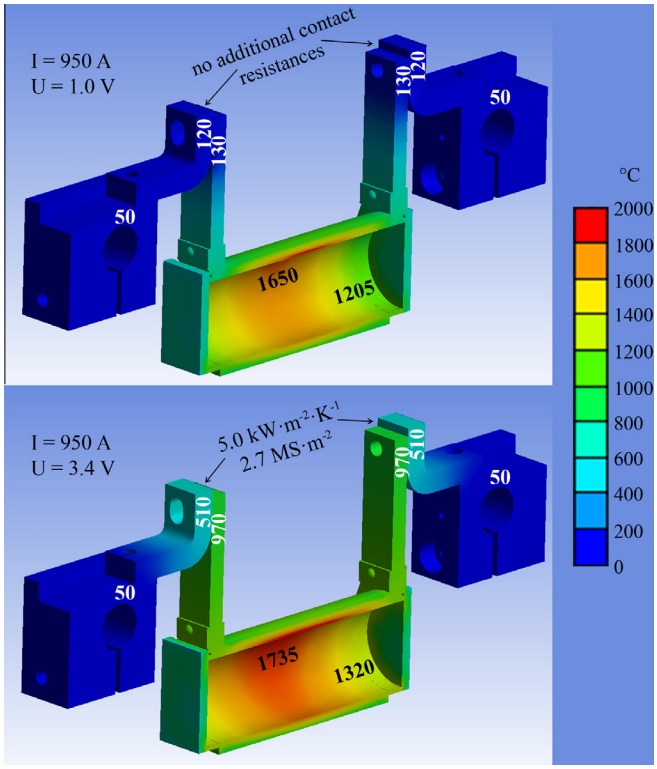

Fig. 4. Thermo-electrical calculations implemented in ANSYS for a heating current of 950 A where the contacts between the Ta sheets and the Cu angle pieces do not produce additional thermo-electric resistances (top) and where the contacts are compromised imposing additional finite heat transfer coefficients and electric conductivities (bottom). Temperatures are given in °C.

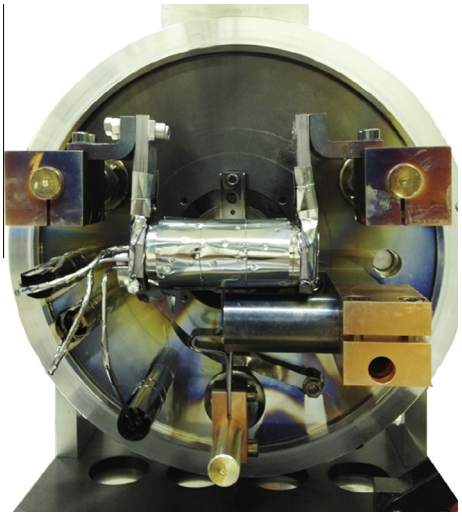

Fig. 5. Prototype target and converter unit #493 without the aluminum vessel.

91–95, 98) and indium (A = 120, 128, 129, 131) have been assessed by using the ISOLDE tape station, equipped with a 4π-beta detector and a high-purity Ge detector for gamma ray spectroscopy. The applicability is versatile, but limited by the branching ratio of the respective decay, the half life of the ion of interest as well as background and detection efficiency. To overcome these limitations, ISOLTRAPs multi-reflection time-of-flight mass separator (MR-TOF MS) has been employed [13]. The MR-TOF MS allows the identification of the isobaric ion species in the ISOLDE beam for isotope-specific yield studies complementary to conventional approaches. With measurement times in the order of 10 ms, direct ion detection and mass-resolving powers in the order of 10^5, this method offers the advantage of not depending on decay properties of the nuclei under investigation. To derive absolute yield numbers of the ISOLDE beam, the efficiency of the ISOLTRAP setup has to be taken into account. In the present case, the MR-TOF MS yields were normalized using the ^{92}Rb beam, the absolute yield of which was measured by beta decay.

Ga, Rb and In were ionized inside of the hot tungsten cavity by surface ionization, while Cu and Zn were ionized by the laser ionization source RILIS [14]. One shall note that the operation of the laser ion source requires in most cases the use of the hot ionizer cavity at the same time, which causes the surface ionized isobaric contamination.

The measured yields, which have been normalized to the primary proton current, of 1×10^{13}–2×10^{13} protons per pulse, are summarized in Table 1. The yields of Zn and Rb will serve for discussion and evaluation of the numerical results. The experimental results for Ga, In and Cu isotopes are given for completeness only, as they have been obtained without optimization of the target and converter unit and shall therefore not be taken as reference. Overall the release efficiencies are low for most isotopes investigated from this unit, which can be accounted to the conservative temperatures adopted during operation of this prototype.

The pulsed nature of the CERN-PSB proton beam allows for time-dependant isotope release measurements. This release curve is commonly approximated by the following four parameter, triple exponential delay function [15]:

Table 1
Experimental yields and calculated in-target production rates based on FLUKA and ABRABLA + TALYS, respectively. The experimental values are assessed by either beta (β) or gamma ray (γ) detection in the ISOLDE tape station or by using the ISOLTRAP MR-TOF MS (I).

Isotope	$T_{1/2}$ (s)	Experimental yield (μC^{-1})	Calculated in-target production rates	
			FLUKA (μC^{-1})	ABRABLA + TALYS (μC^{-1})
^{80}Rb	30	$\leqslant 90^{\gamma}$	2.6×10^{3}	2.3×10^{4}
^{82}Rb	76.2	3000^{β}	6.8×10^{4}	1.2×10^{5}
^{84}Rb	2.83×10^{6}	4.2×10^{4I}	5.1×10^{5}	3.5×10^{5}
^{86}Rb	1.62×10^{6}	1.5×10^{5I}	2.5×10^{6}	8.4×10^{5}
^{88}Rb	1038	$1.3\times10^{6\beta}$	1.3×10^{7}	2.1×10^{6}
^{91}Rb	58	$3.6\times10^{6\beta}$	2.1×10^{8}	1.8×10^{7}
^{92}Rb	4.5	$3.6\times10^{6\beta}$	3.1×10^{8}	9.0×10^{7}
^{93}Rb	5.8	$5.9\times10^{6\beta}$	4.8×10^{8}	1.7×10^{8}
^{94}Rb	2.69	$5.4\times10^{6\beta}$	4.2×10^{8}	2.3×10^{8}
^{95}Rb	0.377	$5.3\times10^{5\beta,\gamma}$	2.7×10^{8}	4.3×10^{8}
^{98}Rb	0.114	$5.8\times10^{3\beta}$	1.5×10^{7}	4.2×10^{7}
^{74}Zn	96	$1.1\times10^{4\beta}$	1.6×10^{6}	5.5×10^{5}
^{75}Zn	10.2	$1.8\times10^{4\gamma}$	1.5×10^{6}	4.9×10^{5}
^{76}Zn	5.6	$4.0\times10^{4\beta,\gamma}$	2.6×10^{6}	4.5×10^{5}
^{78}Zn	1.47	$1.3\times10^{4\beta}$	2.3×10^{6}	1.2×10^{6}
^{80}Zn	0.537	$5.4\times10^{3\gamma}$	8.9×10^{5}	2.5×10^{5}
^{81}Zn	0.29	$4.0\times10^{2\beta,\gamma}$	2.0×10^{5}	3.1×10^{5}
^{80}Ga	1.7	$1.2\times10^{2\gamma}$	1.3×10^{7}	4.1×10^{6}
^{81}Ga	1.22	$1.5\times10^{2\beta}$	1.2×10^{7}	5.9×10^{6}
^{120}In	47.3	$1.5\times10^{4\gamma}$	2.1×10^{8}	4.9×10^{6}
^{128}In	0.84	$4.4\times10^{3\gamma}$	6.3×10^{7}	9.0×10^{7}
^{129}In	0.61	$1.1\times10^{3\gamma}$	4.2×10^{7}	5.9×10^{7}
^{71}Cu	19.5	$1.2\times10^{3\beta}$	3.0×10^{6}	3.2×10^{5}
^{74}Cu	1.594	$2.2\times10^{2\beta}$	1.8×10^{6}	1.4×10^{5}
^{75}Cu	1.224	$9.6\times10^{1\beta}$	2.1×10^{6}	1.7×10^{5}
^{77}Cu	0.469	$3.0\times10^{1\beta}$	8.5×10^{5}	5.3×10^{4}

$$p(t) = \frac{1}{N}\left(1 - e^{-\lambda_r \cdot t}\right)\left(\alpha e^{-\lambda_f \cdot t} + (1-\alpha)e^{-\lambda_s \cdot t}\right) \quad (1)$$

where $p(t)$ is the delay function describing the probability that a radioactive isotope produced by the protons at $t = 0$ is released at time t. λ_r, λ_f and λ_s are the exponential rise, fast fall and slow fall time constants, respectively, and α a weighting factor between the slow and fast components. The factor $\frac{1}{N}$ serves for normalizing $p(t)$ to unity for $t \to \infty$. The decay-constant $\left(\lambda_i = \frac{\ln 2}{T_{1/2}}\right)$ dependant release efficiency, $\varepsilon_{\mathrm{rel}}(\lambda_i)$, of a specific element can be calculated by folding the delay function with the nuclear decay function [16]:

$$\varepsilon_{\mathrm{rel}}(\lambda_i) = \int_{t=0}^{\infty} p(t) e^{-\lambda_i t}\, dt \quad (2)$$

For isotopes of sufficiently long half-lives, $p(t)$ can be derived directly by fitting the experimental release curve. In cases where λ_i is much larger (short half life) than the time constant of the release process (λ_s) there is a large error associated to the release parameters and thus, the decay function needs to be considered in the fitting procedure. Computing the integration using Eqs. 1 and 2 yields to the expression:

$$\varepsilon_{\mathrm{rel}}(\lambda_i) = \frac{1}{N}\left(\frac{\alpha}{\lambda_f + \lambda_i} + \frac{1-\alpha}{\lambda_s + \lambda_i} - \frac{\alpha}{\lambda_f + \lambda_r + \lambda_i} - \frac{1-\alpha}{\lambda_s + \lambda_r + \lambda_i}\right) \quad (3)$$

Fig. 6 shows a comparison between the experimental yields with the simulated in-target production rates, using the FLUKA and ABRABLA + TALYS codes, for different Zn and Rb isotopes. The curves present a bell shape evolution with the highest yields observed in the neutron-rich region for all cases. The evolution of the values is nearly identical in the experimental and in the FLUKA simulated data. The data obtained with ABRABLA + TALYS exhibit a kink in the mass range A = 73–78 for Zn and A = 85–95 for Rb isotopes, which is not observed in the experimental data nor in the yields predicted using FLUKA. A large decrease of the ^{80}Rb yield is observed with a yield of less than 90 ions μC^{-1} in the prototype configuration in contrast to 1×10^5 ions μC^{-1} in the standard converter configuration [5], showing an improvement in the suppression by a factor 10^3. Furthermore, compared to [5], the experimental ^{80}Zn/^{80}Rb ratio is found to be greatly improved by a factor 200 due to the drastic reduction of the contaminant yield.

The calculated values refer to the in-target production rates whereas the experimental data have been obtained after the nuclei diffused from the target, effused to the ion source, were ionized, mass-separated and transported to the detection system. Since each of the mentioned processes has an associated efficiency, the experimental yields will be lower than the in-target production values. The experimental yield (Y_{exp}) can be obtained by multiplying the in-target production ($Y_{\mathrm{in\text{-}target}}$) with the efficiencies associated to the different processes (release, ionization, transport, detection), following the equation:

$$\begin{aligned} Y_{\mathrm{exp}} &= Y_{\mathrm{in\text{-}target}} \cdot \varepsilon_{\mathrm{rel}} \cdot \varepsilon_{\mathrm{ion}} \cdot \varepsilon_{\mathrm{trans}} \cdot \varepsilon_{\mathrm{det}} \\ &= Y_{\mathrm{in\text{-}target}} \cdot \varepsilon_{\mathrm{rel}} \cdot \varepsilon_{\mathrm{o}} \end{aligned} \quad (4)$$

ε_{o} summarizes all contributing losses from the production of the isotope until its detection to one overall efficiency excluding the half-life dependant release efficiency $\varepsilon_{\mathrm{rel}}$ that can be approximated experimentally using Eq. 3. ε_{o} is kept as free parameter to match the experimental release parameters to the simulated data by minimizing the sum of the squared relative differences on a logarithmic scale.

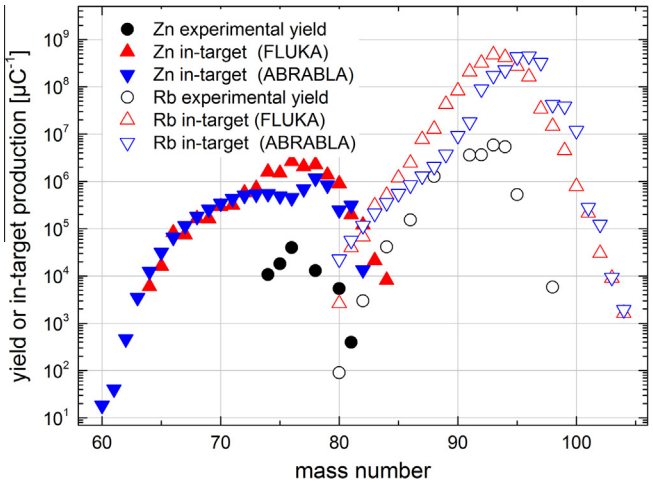

Fig. 6. Experimental yields (circles) and simulated in-target production rates (triangles) for Zn (closed symbols) and Rb (open symbols) isotopes.

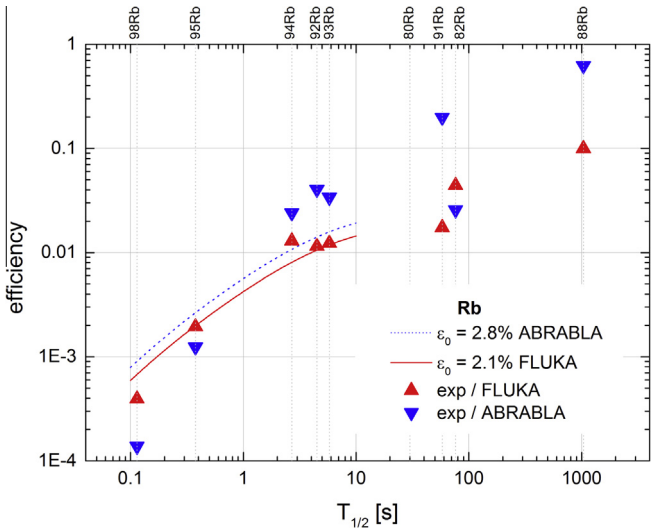

Fig. 7. Efficiency $\varepsilon = \varepsilon_{\mathrm{rel}} \cdot \varepsilon_{\mathrm{o}}$ for Rb isotopes as a function of the isotope half-lives. The experimental release parameters used in the approximation are: α = 0.471, λ_f = 1.82 s^{-1}, λ_s = 0.140 s^{-1} and λ_r = 57.8 s^{-1}.

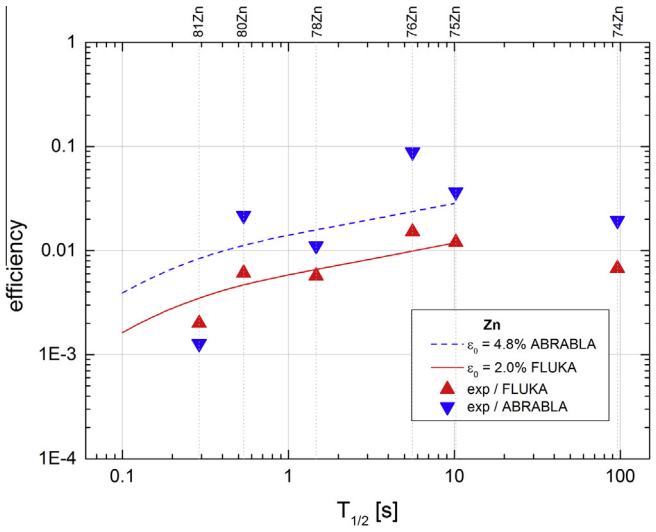

Fig. 8. Efficiency $\varepsilon = \varepsilon_{\mathrm{rel}} \cdot \varepsilon_{\mathrm{o}}$ for Zn isotopes as a function of the isotope half-lives. The experimental release parameters used in the approximation are: $\alpha = 0.968$, $\lambda_f = 3.07$ s^{-1}, $\lambda_s = 0.0507$ s^{-1} and $\lambda_r = 27.7$ s^{-1}.

Figs. 7 and 8 show the calculated efficiencies for Rb and Zn isotopes, respectively. Points illustrate the ratio between the experimentally deduced yields and the different simulated in-target production rates. The lines represent the release function, which is found by fitting the experimental distribution of the isotope release (Eq. 3) for ^{93,95}Rb and ^{76,78}Zn respectively, to the calculated values by introducing a single overall efficiency $\varepsilon = \varepsilon_{rel} \cdot \varepsilon_{o}$, evaluating all contributing losses. Since the experimental release curves were assessed for time constants shorter than 10 s the fitting curve is not presented for longer half lives. For most isotopes, the yields obtained with FLUKA are closer to the experimental data than the ones obtained with ABRABLA + TALYS for both Rb and Zn cases. The larger deviation from the ABRABLA values is consistent with the kink observed in the in-target production yields.

As described earlier, the Rb ionization and release efficiencies are low compared to other ISOLDE production units. However, even if a factor 20 is applied, in order to match the results to efficiencies observed in conventional target units, the ^{80}Zn/^{80}Rb ratio is still greatly enhanced in comparison to standard converter operation.

4. Summary

In this work, an advanced neutron converter design was presented together with experimental results from the assessment of radioactive isotopes production. The prototyped unit was a result of a simulation-based design development, an approach that was successfully validated at ISOLDE with 1.4 GeV proton beam impinging on the new converter. This observation justifies further developments towards an improved target integration around the neutron converter and more sophisticated thermo-mechanical assemblies, aiming at higher production rates and beam intensities without compromising the enhanced suppression factors. A suppression of the order of 10^3 in the contaminant ^{80}Rb yield has been observed, in comparison to the conventional converter configuration. Taking the investigated release efficiency into account, this suppression matches the prediction from simulations. The experimentally derived release efficiencies shows a better agreement with the FLUKA simulations and the experimental data for all measured isotopes than with the ABRABLA + TALYS code. The origin of this result is presently under investigation.

Acknowledgements

The authors would like to acknowledge the support from E. Barbero in the construction of the unit. A. Gottberg acknowledges the financial support of the European Community under the ENSAR-JRA2 ActiLab (Contract Number 262010). R. Luis acknowledges the FCT for PhD Grant No. SFRH/BD/60255/2009. The authors thankfully acknowledge the computer resources, technical expertise and assistance provided by CENTRA/IST. Computations were performed at the cluster "Baltasar-Sete-Sóis", supported by the DyBHo256667 ERC Starting Grant.

References

[1] J. Nolen, Proceedings of the Third International Conference on Radioactive Nuclear Beams, East Lansing, Michigan, USA, May 24–27, 1993.
[2] M. Portillo et al., Nucl. Instrum. Methods Phys. Res. B 194 (2002) 193.
[3] R. Catherall et al., Nucl. Instrum. Methods Phys. Res. B 204 (2003) 235.
[4] E. Kugler, Hyperfine Interact. 129 (2000) 23.
[5] U. Köster et al., AIP Conf. Proc. 798 (2005) 315.
[6] G. Battistoni et al., AIP Conf. Proc. 896 (2007) 31.
[7] A. Fasso et al., Yellow, Report CERN-2005-010, 2005.
[8] A. Koning et al., TALYS 1.2: A Nuclear Reaction Program, USER MANUAL.
[9] A. Junghans, Nucl. Phys. A 531 (1998) 635.
[10] J.-J. Gaimard et al., Nucl. Phys. A 351 (1991) 709.
[11] R. Luis et al., Eur. Phys. J. A 48 (2012) 90.
[12] ANSYS, Academic Research, Release 14.0, Coupled Field Analysis Guide, Ansys Inc.
[13] R.N. Wolf et al., Int. J.Mass Spectrom. 123 (2013) 349.
[14] V. Fedoseyev et al., Hyperfine Interact. 127 (2012) 409.
[15] J. Lettry et al., Nucl. Instrum. Methods Phys. Res. B 126 (1997) 170.
[16] R. Kirchner, Nucl. Instrum. Methods Phys. Res. B 70 (1992) 186.